Earth Sciences
2019; 8(4): 228-234
http://www.sciencepublishinggroup.com/j/earth
doi: 10.11648/j.earth.20190804.12
ISSN: 2328-5974 (Print); ISSN: 2328-5982 (Online)

Behaviors of Converted Wave in an Azimuthally Isotropic Medium - A Physical Model Study

Chih-Hsiung Chang[1, *], Young-Fo Chang[2], Hsiu-Chi Tsao[2]

[1]Department of Biomechatronic Engineering and Research Center for Automation, Chiayi, Taiwan, R. O. C.

[2]Institute of Seismology, National Chung Cheng University, Chiayi, Taiwan, R. O. C.

Email address:

charles@mail.ncyu.edu.tw (Chih-Hsiung Chang), seichyo@ccu.edu.tw (Young-Fo Chang), tsaohsiuchi@gmail.com (Hsiu-Chi Tsao)

[*]Corresponding author

To cite this article:

Chih-Hsiung Chang, Young-Fo Chang, Hsiu-Chi Tsao. Behaviors of Converted Wave in an Azimuthally Isotropic Medium - A Physical Model Study. *Earth Sciences.* Vol. 8, No. 4, 2019, pp. 228-234. doi: 10.11648/j.earth.20190804.12

Received: August 7, 2019; **Accepted**: September 4, 2019; **Published**: September 20, 2019

Abstract: The existence of subsurface fractures provides not only space for the residence of petroleum but also paths of migration. Therefore, subsurface fractures are of great interest to exploration geophysicists. In reflection seismology, a reservoir of vertically aligned fractures is often considered to possess azimuthal anisotropy, or Horizontal Transverse Isotropy (HTI), in terms of seismic anisotropy. The characteristics and information of this specific type of reservoir are widely obtained using seismic attributes, including the azimuthal variation in the *P*-wave amplitude and velocity, and the fractional difference of split *S*-waves. Essentially, a converted (*C*-) wave is initiated by a downward traveling *P*-wave, which is converted on reflection to upcoming *S*-waves. Hence, it combines the behaviors of *P*- and *S*-waves in theory. Using a forward model study, this study demonstrates the behaviors of a *C*-waves in a HTI medium, instead of the behaviors of *P*- or *S*-waves. Reflections are facilitated on the horizontal symmetry-axis plane of a scaled HTI model along seven different azimuths using end-on shooting arrangement. Using a *P*-type transducer as a source and an *S*-type transducer as a receiver, the behaviors of *C*-waves in a HTI medium are observed. In the acquired profiles, reflections of *P*-, PS_1- (C_1-), and a mixture of PS_2- (C_2-) and S_1-waves were detected. The phenomenon of *C*-wave splitting is also observed because of the behavior of an *S*-wave in a Transversely Isotropic Medium (TIM), and it could be easily identified in the azimuths near the fracture plane. The reflectivity strengths obtained using a Hilbert transform show that the azimuthal variation in the Amplitude Versus Offset (AVO) for both *P*- and C_1-waves are consistent, but the C_1-wave amplitude variation depends more significantly on the azimuth than that of the *P*-wave. Furthermore, the percentage anisotropy of the *C*-wave computed from acquired data falls right between those of *P*- and *S*-waves. By incorporating *C*-wave splitting and azimuthal AVO variation into traditional signature analyses, our results show that the fracture orientation is more pronounced when the potential reservoir has vertically aligned fractures.

Keywords: Anisotropy, Converted Wave, Splitting, Amplitude Versus Offset

1. Introduction

Subsurface fractures are of geophysical interest [1, 2] because fractures in subsurface formations increase permeability and porosity for hydrocarbon flow and residence. In natural processes, fractures are commonly caused by stress. The state of stress is anisotropic and significantly related to the dominant fracture orientation and fracture density. The in-situ anisotropy imparts important reservoir properties that are related to fractures and stress fields [3]. In petroleum engineering, to optimize production and reservoir drainage, directional drilling must be oriented perpendicular to the alignment of the fractures. For vertical fractures, holes must be drilled in areas of high fracture density [4].

Traditionally, information on fractured reservoirs is obtained using seismic attributes, including azimuthal variations in *P*-wave velocity and amplitude and the time difference between the mutual orthogonal polarizations of split *S*-waves. In seismic anisotropy, a reservoir composed of systematically aligned vertical fractures with a horizontal symmetry axis is often categorized as a horizontal transverse isotropy (HTI) [5]. For a fractured reservoir with the characteristics of an HTI, the interval velocity of *P*-waves

decrease when they pass across a vertical fracture set compared to the velocity parallel to the fracture set [6]. In a combination of azimuthal *P*-wave velocity anomalies and amplitude variation with offset and azimuthally (AVOAz) dependent *P*-wave analyses, fracture swarms can be mapped and fracture orientations in the swarms can potentially be identified [7, 8]. Laboratory and field data and theoretical calculations can also establish a link between the attenuation of *P*-waves and the orientation of open fractures [9, 10]. The existence of fractures also induces *S*-wave splitting; this can be used to access fracture information from a target reservoir. References [7, 11, 12] proposed that the measurements of travel times between split *S*-waves in a single propagation direction be used for definitive anisotropy identification, i.e., determining the direction of the maximum and minimum horizontal stresses and an indication of the difference between them.

With the development of multicomponent seismic acquisition and processing techniques, both *P*- and *S*-wave modes can be used to capture more information on rock properties, such as fracture locations, density, and orientation. The use of *C*-waves in petroleum exploration has also benefitted advances in multicomponent seismic acquisition. Fundamentally, a *C*-wave is initiated by a downward traveling *P*-wave that is converted on reflection to upcoming *S*-waves. Because a *C*-wave is produced by a modal conversion of a *P*- to an *S*-wave, it combines the behaviors of *P*- and *S*-waves. Therefore, *C*-waves contain the signatures of *P*- and *S*-waves used for calculating the magnitude of azimuthal anisotropy and determining the orientation of the principal axis of a fractured reservoir. In addition, combined *P*- and *C*-wave data can provide more reliable information of a subsurface fractured system than from combined *P*- and *S*-wave data analysis. This is because *C*-wave data often yield better resolution and better signal-to-noise, compared to SS data [13].

Exploiting the *C*-wave amplitude variation with offset (AVO) to determine the physical properties, especially the orientation and density variation of subsurface fractures, and estimate the elastic properties of lithology is becoming increasingly popular in reflection seismology [14, 15]. Here, a forward model study was carried out to gain more detailed insights into the splitting of *C*-waves [16] and the difference in travel time between split *C*-waves [17, 18] and AVOAz [19]. To explore the behaviors of *C*-wave in an azimuthally isotropic medium, seven end-on shooting reflection experiments were conducted in the horizontal symmetry axis plane of a fractured model in azimuth. Acquired data were processed by the Hilbert transform to analyze the reflection strengths of relative events in post-operation. The laboratory results clearly demonstrated the expected observations.

2. Laboratory Work

Fractured Model–Horizontal Transverse Isotopy (HTI) Block

Phenolite is a resin of interlaced paper and woven fiber. Thus, because of its layered composition, phenolite is used to study the behaviors of elastic wave propagation in a TIM or an orthorhombic material [20, 21, 22, 23, 24]. The phenolite used in this study exhibited the characteristics of TIM and has elastic constants normalized by density (1.4×10^3 kg⁄m^3) as follows: $A_{11} = 16.56$, $A_{13} = 4.47$, $A_{33} = 8.46$, $A_{44} = 2.16$, and $A_{66} = 4.73$ ($\times 10^6$ m^2⁄s^2) [25, 26]. The percentage anisotropy [27] of the *P*- and *S*-waves obtained from premeasured elastic constants were 33.3 and 38.7, respectively. To relate more directly to seismic data, these five independent constants are often combined into Thomsen parameters: $\varepsilon = 0.48$, $\gamma = 0.59$, and $\delta = 0.04$ [28]. To facilitate our objective, a scaled model with dimensions 80 mm (L) × 80 mm (W) × 60 mm (H) was machined from a phenolitic block. The symmetry axis of the machined block was horizontally oriented and behaved as a fractured (HTI) model (Figure 1(a)).

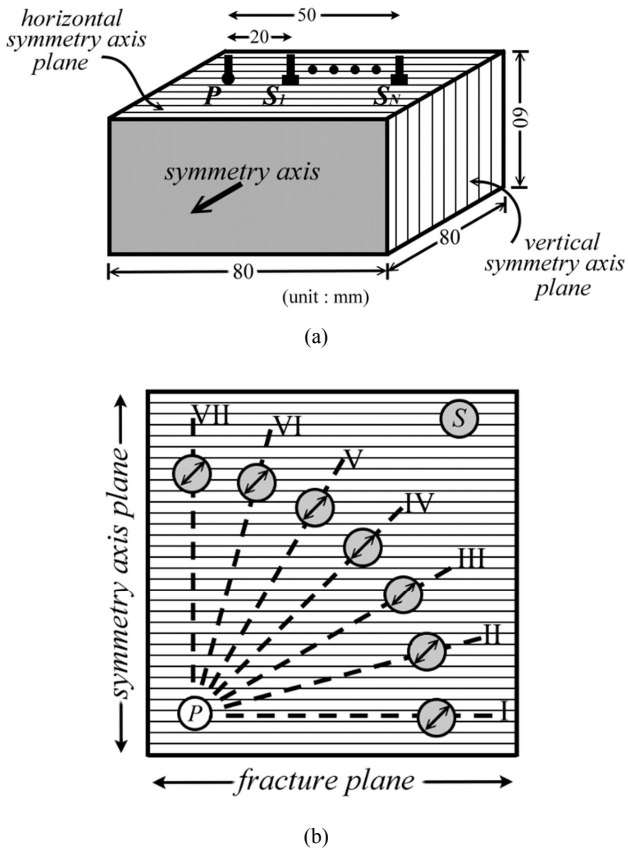

Figure 1. *Schematic diagrams of (a) the configuration of the fractured (HTI) model and (b) the azimuthal layout of survey lines. Line I runs along the fractured plane and Line VII follows the symmetry axis. Note that the polarization of the S-type is diagonally oriented.*

Experimental Setup

In order to acquire *C*-waves originating from a modal conversion, acoustic energy in the reflection experiments was generated using a longitudinal mode *P*-type transducer (Panametrics A133S, 2.25 MHz, 6 mm) and it was received by a shear mode *S*-type transducer (Ultran SWC50-1, 1 MHz, 13 mm). In the process of data acquisition, both of the active transducers were excited by a Panametrics 5058

pulse-receiver in the double probe mode. Seven end-on shooting reflection experiments were performed in the horizontal symmetry axis plane of the HTI model (Figure 1(b)). The layouts for observation were evenly distributed in the quadrant between the fractured plane and symmetry axis, and the angular interval between successive layouts was 15°. The polarization of the *S*-type transducer was diagonally oriented with respect to either the fractured plane or the symmetry axis during data acquisition. The near and far offsets for the layout were 20 mm and 50 mm, respectively, and the offset interval was 1 mm for each successive measurement. Each observation consisted of 5,000 sampling points, sampled at 8 ns and 40 μs in recorded length. The scaling factor for both time and space was 10,000; i.e., 1 mm and 1 ns were respectively equivalent to 10 m and 10 μs in field operation. The received signals and reflections originating from the interface of phenolite and air were amplified, filtered, and sent to a Tektronix TDS-5032B digital oscilloscope. Finally, the observed signals were digitized and downloaded to a PC486 via IEEE-488 GPIB for further analysis and interpretation.

3. Results and Discussions

Techniques of multicomponent acquisition have significantly contributed to the current development of *C*-wave exploration. In case of isotropy, *C*-wave images reflect the conversion of a downgoing *P*-wave to an upcoming *S*-wave at the deepest point of penetration. However, in the presence of anisotropy, the upcoming *S*-wave splits into two components, which travel with different velocities and have mutually orthogonal polarizations when the direction of propagation deviates from the principal symmetry axis of the anisotropic medium. In a fractured reservoir, the *S*-wave component polarized parallel to the fracture orientation travels at a faster velocity than the transversely polarized component. Considering the origins of *C*-waves, *C*-wave splitting and the azimuthal amplitude variation in *C*-waves can be used to derive the physical properties of a fractured reservoir in prospection.

C-wave splitting

Despite the contribution of multicomponent acquisition techniques, limitations to the arrangement, planting, and the identification of reflected events are operational issues [29]. To overcome the operational limitations in the field, a forward model study was used to demonstrate the behavior of *C*-wave splitting in a "fractured" model. In the laboratory, reflection experiments were performed on the horizontal symmetry axis plane of the phenolitic block with HTI characteristics. From the layering strike to the direction of the symmetry axis, seven end-on shooting reflection profiles with an angular interval of 15° were collected (Figure 1(b)) [30, 31]. The intentional orientation of the polarization of the *S*-type transducer allowed the acquisition of both components of the layering motion: the faster mode PS_1- (C_1-) wave and the in symmetry-axis motion, which is the slower mode PS_2- (C_2-) wave.

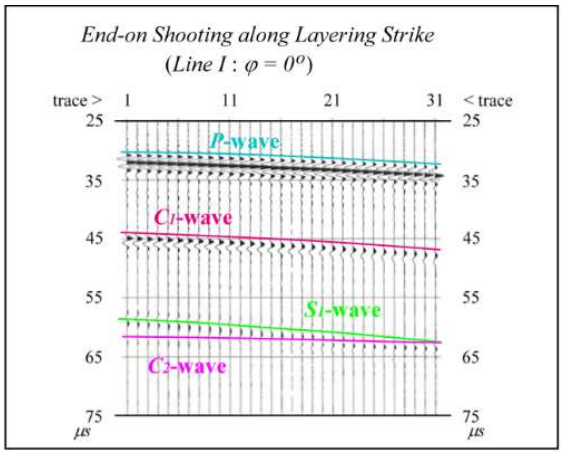

(a)

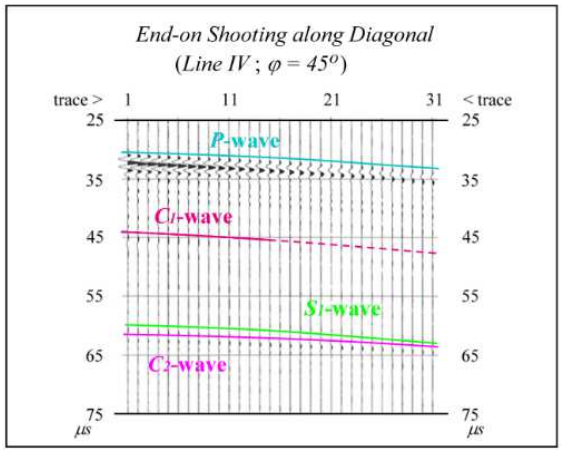

(b)

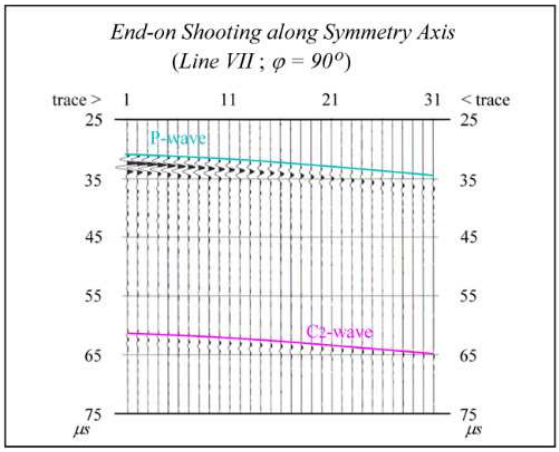

(c)

Figure 2. *End-on shooting profiles acquired along (a) the layering (Line I, φ = 0°), (b) the layering diagonal (Line IV, φ = 45°) and (c) the symmetry axis (Line VII, φ = 90°). A comparison of (a) and (c) shows that reflected PS_1- (C_1-) and S_1-waves observed in (a) are not detected in (c). Only P- and C_2- waves are identified in all acquired profiles.*

In all seven acquired profiles, only *P*-wave reflections were completely detected and identified. Figure 2 shows reflections acquired along the layering strike ($\varphi = 0°$, Figure (2a)), diagonal ($\varphi = 45°$, Figure (2b)), and symmetry axis (φ

= 90°, Figure (2c)). The colored curves delineate the moveouts of *P*-, C_1-, C_2-, and S_1-waves. Apart from *P*-wave reflections, a mixed mode of C_1-, S_1-, and C_2-waves was observed in the layering direction (Figure 2(a)). C_1- and C_2-waves shown in Figure 2(a) were observed at approximately 45 ms and 63 ms and the equivalent C_1- and C_2-wave moveout velocities, computed from the detected arrivals, were 2879 m/s and 1978 m/s, respectively. As expected, the phenomenon of *C*-wave splitting was observed in the layering strike of the HTI model. The variation of AVO was also more significant in the C_1-wave than in the *P*-wave. Although the C_1-, S_1- and C_2-waves are still observable in Figure 2(b), the phenomenon of *C*-wave splitting is only observed when the offset distance is less than 35 mm, i.e. trace 16. The gradual fade out in C_1-waves is clearly shown in Figure 3, which presents a magnified view of S_1- and C_2-waves. In Figure 3(a), the arrival of S_1- and C_2-wave reflections are well separated and can be easily delineated. A comparison of Figure 3(b) and Figure 3(a) shows that the S_1-wave becomes more indistinct in the offset. As S_1-waves become barely detectable after trace 16, C_1-waves from the modal conversion of *P*- to S_1-waves are not observed. In Figure 2(c), the profile shows that of the reflections acquired along the direction of the symmetry axis, only *P*- and C_2-waves are detected. The arrival of S_1-waves is no longer observed (Figures 2(c) and 3(c)) because the S_1- and S_2-waves travel at the same velocity in the symmetry axis. The converted wave, which is labeled a C_2-wave in Figures 2(c) and 3(c), may be a mixed mode of C_1- and C_2-waves. The phenomena of *C*-wave splitting in the azimuth shown in our observations is similar to that described by [30].

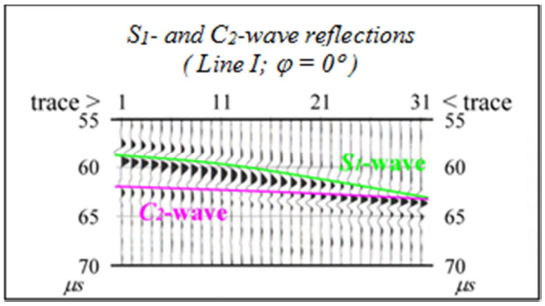

(a)

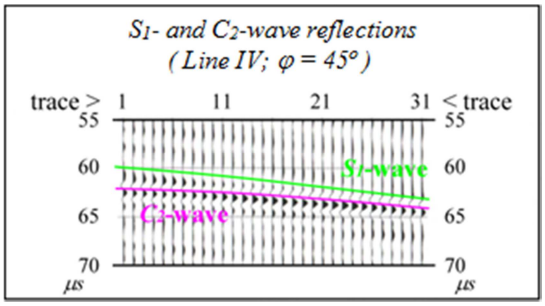

(b)

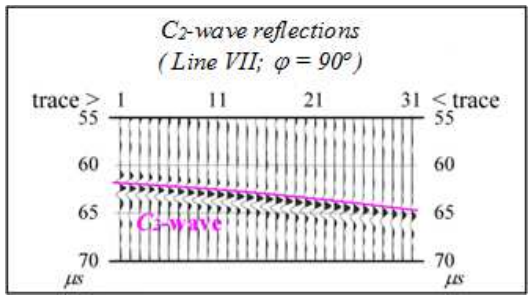

(c)

Figure 3. *Magnified views of S_1- and C_2-waves shown in Figure 2: (a) Layering (Line I, φ = 0°), (b) layering diagonal (Line IV, φ = 45°) and (c) the symmetry axis ((Line VII, φ = 90°).*

Azimuthal AVO variation of C-wave

As stress-induced fractures are closely related to anisotropy, [32] proposed that the orientation and intensity of fractures and stress fields can be determined by analyzing the AVOAz of a *P*-wave. [30] showed that reliable information about a fractured reservoir can be derived by incorporating *C*-wave data into the inversion process. Moreover, the azimuthal variation of *C*-wave amplitude in a fractured reservoir has been demonstrated by [33]. To explore the relationship between the AVOAz of a *C*-wave and the layering orientation of the HTI model or the fracture orientation of a fractured reservoir, end-on shooting reflections acquired from the same horizontal symmetry axis plane but different azimuths were further analyzed using a Hilbert transform [34], and the reflection strengths of the *P*-, C_1-, and C_2-waves were calculated. Figure 4 shows the data for the computed reflection strengths of the C_1- and C_2-waves (or C_1- and mixed mode of C_2-+S_1-waves) at four different offsets. The azimuthal variations in the reflection strengths of the relative events in the near offset traces are shown in Figure 4(a). When observations were made in the azimuths of the fracture orientation (Line I; φ= 0°) to the fracture diagonal (Line IV; φ = 45°), the variation in the reflection strength of the C_1-wave was prominent. The strength of the reflected C_1-wave also shows a consistently weakening trend in Lines I, II and III. The other three constant offset gathers also exhibited a similar trend. However, the attenuation of reflection strengths of the C_1-wave in the azimuth become indistinct as the offset increased. The effect on the AVOAz for the C_1-wave in Lines I, II and III can also be observed through a visual inspection of the relative traces shown in Figure 4.

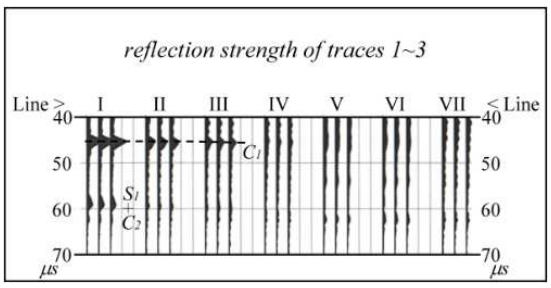

(a)

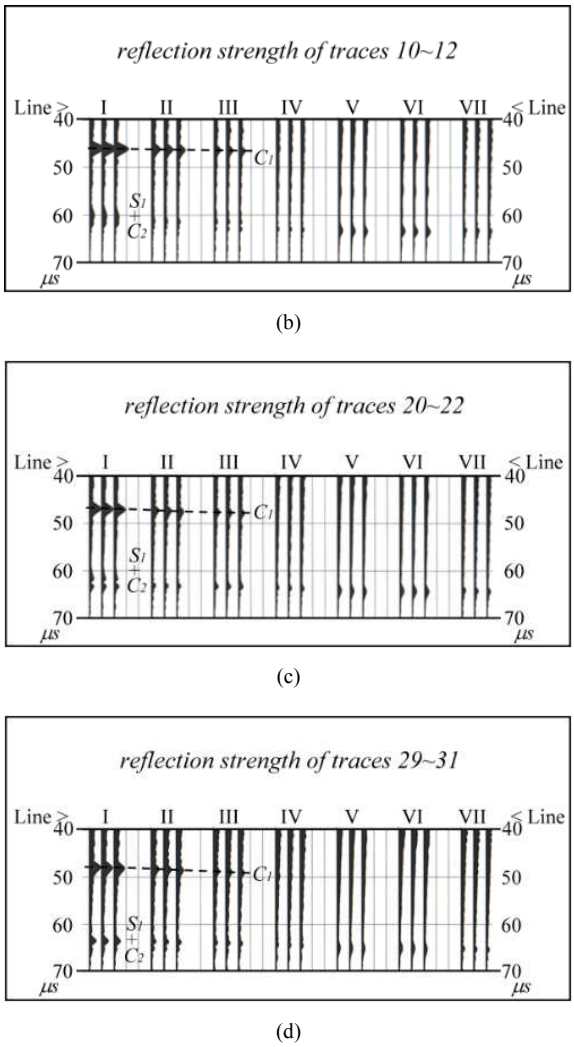

Figure 4. *Strengths of reflections of C_1-, S_1- and C_2-waves or C_1-waves and a mixed mode of S_1- and C_2- waves at four constant offset gathers. The offset interval for (a) trace 1 is 20 mm, (b) trace 11 is 30 mm, (c) trace 21 is 40 mm, and (d) trace 31 is 50 mm.*

Figure 5 shows the behaviors of the AVOAzs of the *P*-, C_1-, and C_2-waves. The data was normalized by the maximum reflection strength of the relative events acquired along the layering strike ($\varphi = 0°$). As shown in Figure 4, the reflection strengths of both *P*- and C_1-waves consistently decreased from the layering strike ($\varphi = 0°$) to the layering diagonal ($\varphi = 45°$) (Figures 5(a) and 5(b)). A comparison of Figures 5(a) and 5(b) shows that the AVO for a C_1-wave is more sensitive to fractures than that of a *P*-wave. These results agree with analytic approximations for reflection coefficients in azimuthally anisotropic media [35]. Because of the haphazard arrival of C_2- and S_1-waves (Figures 3(c) and 3(d)), the reflection strengths of the relative events cannot be confidently isolated and identified. Therefore, the relationship between the AVOAz of C_2-wave and the layering strike (i.e. fracture orientation) is not generalized for the HTI model.

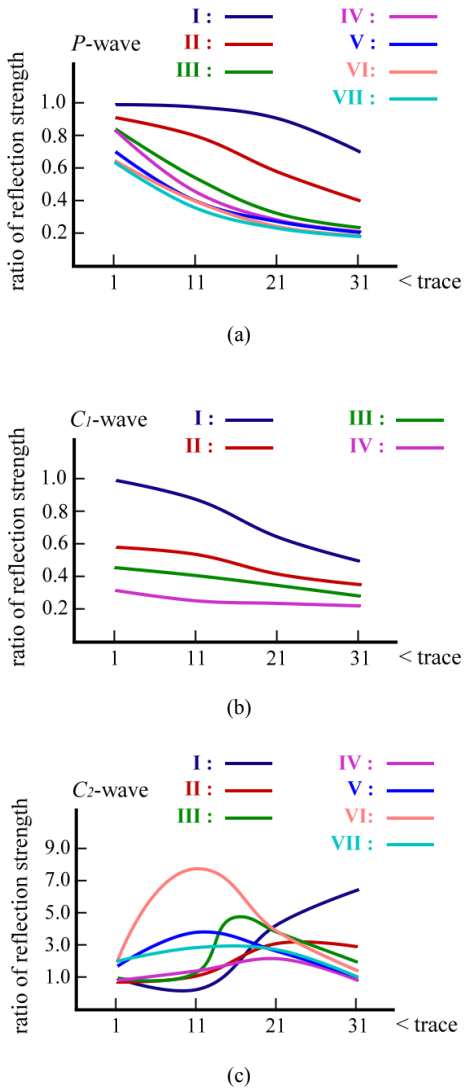

Figure 5. *AVOAzs for (a) the P-wave, (b) C_1-wave and (c) C_2-wave shown in Figure 4. The dark blue curves show the AVO of relative events observed along the fracture orientation ($\varphi = 0°$). It is noteworthy that the attenuation in the AVO for a C_1-wave is more significant than that in a P- wave in fracturing.*

4. Conclusions

The existence of fractures can cause changes in the physical properties of a propagating seismic wave to vary with azimuth. For reflections acquired from the horizontal symmetry-axis plane of a scaled model, *C*-waves were verified to reflect the behaviors of *P*- and *S*-waves. In the laboratory, the birefringence of a *C*-wave was found to be consistent to that of *S*-wave splitting. AVOAz was also observed in *P*- and C_1-waves; however, the latter was more sensitive to fracture orientation. The percentage anisotropy of the *C*-wave computed from laboratory data was 36.6, which falls between the values of 33.3 and 38.7 for *P*- and *S*-waves, respectively. The signatures of *P*- and *S*-waves related to the fracture orientation and intensity in reflection seismology were also observed in *C*-waves. As the variations in velocity and amplitude of *P*-waves and the fractional difference of split *S*-waves are commonly used seismic attributes for assessing

the magnitude of the azimuthal anisotropy and the orientation of the principal axis from a fractured reservoir, these results show that the azimuthal dependence of *C*-wave behaviors can be used in traditional seismic analyses to obtain reliable information from subsurface fractured formations.

Acknowledgements

We wish to express our appreciation to anonymous reviewers for providing very constructive suggestions and comments in revising this paper. Our appreciations also go to Lady Grace Hsu for her valuable effort and time in editing this paper. The research leading to this paper was financially supported by the Ministry of Science and Technology under grant no. MOST 106-2116-M-415-001- and MOST 107-2116-M-415-001 –.

References

[1] Aguilera, R. (1998). Geologic aspects of naturally fractured reservoirs. The Leading Edge 17, 1667-1670.

[2] R. A. Nelson, "Geologic Analysis of Naturally Fractured Reservoirs," Elsevier Inc., 2001.

[3] Williams, M. and E. Jenner (2002). Interpreting seismic data in the presence of azimuthal anisotropy; or azimuthal anisotropy in the presence of the seismic interpretation. The Leading Edge 21, 771-774. https://doi.org/10.1190/1.1503192

[4] Mueller, M. C. (1992). Using shear waves to predict lateral variability in vertical fracture intensity. The Leading Edge 11, 29-35. https://doi.org/10.1190/1.1436870

[5] Tsvankin, I. (1997). Reflection moveout and parameter estimation for horizontal transverse isotropy. Geophysics 62, 614-629.

[6] Chang, C. H. and G. H. F. Gardner (1997). Effects of vertically aligned subsurface fractures on seismic reflections - a physical model study. Geophysics 62, 245-252.

[7] Pérez, M. A., R. L. Gibson, and M. N. Toksöz (1999). Detection of fracture orientation using azimuthal variation of P-wave AVO responses. Geophysics 64, 1253-1265. https://doi.org/10.1190/1.1444632

[8] Treadgold, G., C. Sicking, V. Sublette, and G. Hoover (2008). Azimuthal Processing for Fracture Prediction and Image Improvement. 78th Annual International Meeting, SEG, Expanded Abstracts, 988-992. https://doi.org/10.1190/1.3063803

[9] Maultzsch, S., M. Chapman, E. Liu, and X. Y. Li (2007). Modelling and analysis of attenuation anisotropy in multi-azimuth VSP data from the Clair field. Geophysical Prospecting 55, 627-642.

[10] Ekanem, A. M., J. Wei, X. Y. Li, M. Chapman, and I. G. Main (2013). P-wave attenuation anisotropy in fractured media: A seismic physical modelling study. Geophysical Prospecting 61, 420-433. https://doi.org/10.1111/j.1365-2478.2012.01127.x

[11] Ray, R. R. (2001) S-Waves Detect Reservoir Flows. Explorer, September, 41-42.

[12] Roche, S., M. Wagaman, and H. Watt (2005). Anadarko Basin survey shows value of multicomponent acquisition. First Break 23, 43-52.

[13] Garotta R., C. Vuillermoz, and P. Y. Granger (1990) Comparing 3-D Operations and Results from Converted PS Waves. 60th Annual International Meeting, SEG, Expanded Abstracts, 1086-1088.

[14] Reine C. and R. Tilson (2016). Insights into converted-wave AVO and its use in inversion. GeoConvention: Optimizing Resources.

[15] Sadeghi E., C. Adam, E. Siawira and H. Khairy (2017). P-S Converted wave AVO analysis for reservoir characterization. 41st Annual Convention Proceedings, Indonesian Petroleum Association.

[16] Tsvankin, I. and V. Grechka (2011). Seismology of Azimuthally Anisotropic Media and Seismic Fracture Characterization. Society of Exploration Geophysicists, 372-387. https://doi.org/10.1190/1.9781560802839

[17] Ata, E. and R. J. Michelena (1995). Mapping distribution of fractures in a reservoir with P-S converted waves. The Leading Edge 14, 664-676.

[18] Gaiser, J. E. and R. Van Dok (2005). Multicomponent processing and fracture characterization analysis of 3-D PS-wave onshore seismic surveys. Society of Petroleum Engineers. https://doi.org/10.2118/93740-MS

[19] Sun, J. and K. Innanen (2014). A review of converted wave AVO analysis. CREWES Research Report (26), 1-13.

[20] Chang, C. H., G. H. F. Gardner, and J. A. McDonald (1994). A physical model study of shear-wave propagation in a transversely isotropic solid. Geophysics 59, 484-487.

[21] Okoye, P. N., N. F. Uren, and W. Waluyo (1995). Variation of stacking velocity in transversely isotropic media. Exploration Geophysics 26, 431-436.

[22] Waluyo W., N. F. Uren, and J. A. McDonald (1995). Poisson's ratio in transversely isotropic media and its effects on amplitude response: an investigation through physical modeling experiments. SEG Technical Program Expanded Abstracts, 585-588.

[23] Grechka, V., S. Theophanis, and I. Tsvankin (1999). Joint inversion of P- and PS-waves in orthorhombic media: Theory and a physical-modeling study. Geophysics 64, 146-161.

[24] Mah, M. and D. R. Schmitt (2001). Experimental determination of the elastic coefficients of an orthorhombic material. Geophysics 66, 1217-1225.

[25] Chang, Y. F. and C. H. Chang (2001). Laboratory Results for the Features of Body Wave Propagation in a Transversely Isotropic Medium. Geophysics 66, 1921-1924.

[26] Chang, Y. F., M. C. Chou, C. H. Chang (2006). Experimental measurements of the phase and group velocities of body waves in a transversely isotropic medium. NDT&E International 39, 162-168.

[27] Barclay A. H. and D. R. Toomey (2003). Shear wave splitting and crustal anisotropy at the Mid-Atlantic Ridge, 35°N. Journal of Geophysical Research 108, EPM 2-1~2-8. https://doi.org/10.1029/2001JB000918

[28] Thomsen, L. (1986). Weak elastic anisotropy. Geophysics 51, 1954-1966.

[29] Stewart R. R., J. E. Gaiser, R. J. Brown, and D. C. Lawton (2002). Converted‐wave seismic exploration: Methods. Geophysics 67, 1348-1363. https://doi.org/10.1190/1.1512781

[30] Bale, R., B. Gratacos, B. Mattocks, S. Roche, K. Poplavskii, and X. Li (2009). Shear wave splitting applications for fracture analysis and improved imaging: some onshore examples: First Break 27, 73-83.

[31] Mattocks, B., J. Li, and S. L. Roche (2005). Converted-wave azimuthal anisotropy in a carbonate foreland basin. SEG Technical Program Expanded Abstracts, 897-900. https://doi.org/10.1190/1.2148304

[32] Stewart R. R., J. E. Gaiser, R. J. Brown, and D. C. Lawton (1999). Converted-wave seismic exploration: a tutorial. CREWES 11 (3).

[33] Chang, C. H., Y. F. Chang, P. Y. Tseng (2017). Azimuthal variation of converted-wave amplitude in a reservoir with vertically aligned fractures a physical model study. Geophysical Prospecting 65, 221-228.

[34] R. N. Bracewell, “The Fourier transform and its application,” McGraw-Hill Book Co., Inc., 1986, pp 268-271.

[35] Rüger, A. (1998) Variations of P-wave reflectivity with offset and azimuth in anisotropic media. Geophysics 63, 935-947.